TiO$_2$ (rutile and anatase) deposited on ordered mesoporous SiO$_2$: effect of pore size on photocatalytic activity

Azadeh Haghighatzadeh[a,*], Babak Mazinani[b], Mehdi Shahedi Asl[c], Leila Bakhtiari[d]

[a]*Physics Group, Department of Sciences, Ahvaz Branch, Islamic Azad University, P.O. Box 61349-68875, Ahvaz, Iran,*
Tel. +98 9122935223; email: azadeh.haghighatzadeh.physics@gmail.com
[b]*Department of Materials Engineering, Malayer University, Malayer, Iran, Tel. +98 9122935223; email: b.mazinani@gmail.com*
[c]*Department of Mechanical Engineering, University of Mohaghegh Ardabili, Ardabil, Iran,*
Tel. +98 9123277186; email: mehdi.shahedi@gmail.comx
[d]*SHEZAN Research and Innovation Center, Pardis Technology Park, Tehran 1657167333, Iran,*
Tel. +98 9123198645; email: lbakhtiari@Shezan.ir

a b s t r a c t

The aim of the study is to show how the pore size of mesoporous SiO$_2$ host structures can affect the physical and photocatalytic properties of the impregnated host structure with TiO$_2$ nanoparticles. The first phase of the investigation involved preparing mesoporous silica structures at two different hydrothermal temperatures (70°C and 130°C) which resulted in achieving different pore sizes in each sample. The synthesized samples were then impregnated with TiO$_2$ nanoparticles (rutile and anatase) and finally heat treated at two different temperatures (400°C and 800°C). The prepared materials were characterized by X-ray diffraction, small-angle X-ray scattering, N$_2$ adsorption–desorption isotherm measurements, transmission electron microscopy and UV–Vis spectroscopy. After calcination of impregnated samples at a low temperature (400°C), the sample with higher surface area (365 m^2/g) showed a photoactivity half as big as the sample with lower surface area (329 m^2/g). This phenomenon is due to the effect of pore size on localization of TiO$_2$ nanoparticles (rutile and anatase) inside the pores and consequently on photocatalytic properties. In fact, since large rutile crystals can enter the channels of samples with large pores, coexistence of rutile and anatase crystals can lead to more photocatalytic efficiency. All of the samples indicated higher photoactivity with increased calcination temperature from 400°C to 800°C due to an increasing degree of crystallinity. Interestingly, the sample with larger pores retained a higher surface area and pore volume compared with the sample having smaller channels at elevated temperatures (800°C) owing to the existence of open and accessible pores.

Keywords: Mesoporous; TiO$_2$; Sol–gel; Pore size; Photocatalytic activity

1. Introduction

Over the last few years, using titanium oxide due to its photocatalytic properties for degradation of organic pollutants and dyes has attracted the attention of researchers [1,2]. Photoactivity of TiO$_2$ crystals can be affected by several parameters including surface area, phase combination, crystallinity and additives [3–7]. Testino et al. [8] reported that particle morphology and surface chemistry are two important factors as well. As photoactivity can be enhanced by increasing the surface area of TiO$_2$ particles, many researches have done this to achieve TiO$_2$ with small particle sizes. However, the separation of nanopowder TiO$_2$ can be considered as a difficult industrial process from liquid or gas. Thus, some scientists have tried to synthesize mesoporous TiO$_2$ in order to gain high surface area and large particles simultaneously [9].

* Corresponding author.

Nevertheless, the preparation of mesoporous TiO_2 due to a high reaction rate of Ti-precursors and low thermal stability of TiO_2 particles is not an easy and economical solution [10,11]. As a result, some researchers have focused on anchoring TiO_2 nanoparticles on various materials, such as zeolites, silicas and carbon materials [5,12–15].

Since the discovery of the mesostructured silica family [16], the incorporation of TiO_2 nanoparticles with mesostructured silica has attracted the focus of scientists because of their large surface area and pore volume. This has resulted in many investigations regarding the effects of synthesis parameters on the photocatalytic efficiency of mesoporous SiO_2–TiO_2 [5,6,17,18].As reported, titania–silica mixed oxide not only enhances the activity and surface acidity of TiO_2 [19] but also improves the thermal stability of anatase phase [20]. Reitz et al. [9] have shown that anatase-to-rutile transformation does not occur below 800°C [9]. This makes titania–silica (TiO_2/SiO_2) binary mixed oxide an appropriate alternative for industrial usage. Many researchers reported that the formation of Ti–O–Si bonds improve the photoactivity of the composite due to an increase in Bronsted acidity on the surface of material [21,22]. Mazinani et al. [5] stated that the surface area and degree of crystallinity are two effective factors on the photocatalytic efficiency of mesoporous TiO_2–SiO_2 when TiO_2 exists as an anatase phase in the composite. Su et al. [23] reported that mesocellular foams (MCF) as a host structure improves the photoactivity compared with SBA-15 due to the large pores of MCF.

It has been observed that the coexistence of rutile and anatase crystals beside each other improves photocatalytic properties [7,18]. Su et al. [23] showed that a titania film of anatase–rutile has a higher photoreactivity compared with pure anatase. Recently, Wang et al. [24] have reported that the rutile to anatase ratio is an important parameter as well. Regarding the mesoporous TiO_2–SiO_2 composite, TiO_2 nanoparticles should be incorporated into the channels of the silica host structure. Due to the different crystal sizes of rutile and anatase, it is expected that the pore size of ordered mesoporous SiO_2 shows an important role in the dispersion of TiO_2 particles into the mesoporous channels and consequently in photoactivity.

In this study, we first prepared ordered mesostructure SiO_2 with different pore sizes by changing the hydrothermal temperature. The rutile and anatase phases were then introduced to the prepared samples, which were then heat treated at different temperatures. Finally the synthesized samples were evaluated in terms of structural and photocatalytic properties.

2. Material and methods

2.1. Chemicals

Pluronic P-123 $(HO(CH_2CH_2O)_{20}(CH_2CH(CH_3)O)_{70}(CH_2CH_2O)_{20}H)$ (MW = 5800) and Titanium isopropoxide (TTIP) were obtained from Sigma-Aldrich (Germany). Tetraethyl orthosilicate (TEOS) and HCl (37% concentration) were purchased from Merck (Germany). Methylene blue (MB) (>97%) was bought from Sigma-Aldrich and P25 titanium dioxide (anatase 80%, rutile 20%, surface area 50 m^2/g and particle size 27 nm) was purchased from Degussa (Germany).

2.2. Synthesis method

2.2.1. Support

In a typical synthesis procedure, 4 g of P123 was dissolved in a solution of water (30 g) and 2 M HCl (120 g), and the mixture was stirred for 5 h at 40°C. Following this, 9 g of TEOS was introduced to the solution while stirring. After stirring the solution for 24 h, the mixture was transferred to a Teflon-lined autoclave and heat treated at 70°C and 130°C for 48 h. The prepared materials were filtered, washed and dried. The resulting powders were then calcined at 540°C to remove organic parts. The resulting materials are designated Sx, where x is the hydrothermal temperature.

2.2.2. Post-modification

The post-modification of prepared mesoporous SiO_2 host structure was based on the sol–gel procedure [18,25]. At first, TTIP (weight ratio of SiO_2/TiO_2 = 2) was added to 1 M HNO_3 solution (30 mL) with continuous stirring for 2.5 h at 70°C. Then, the mixture was diluted with 50 mL of water and the pH of the solution was then adjusted to 3 with 1 M NaOH. At pH 3, there is an electrostatic interaction between the positively charged TiO_2 particles and the negatively charged SiO_2 host material. Afterwards, the prepared mesoporous SiO_2 was added to the mixture and it was stirred for 2 h at 70°C. The resulting materials were filtered, washed, dried and heat treated at 400°C and 800°C for 3 h. The obtained samples are designated as Sx-y, where x and y are the hydrothermal and calcination temperatures, respectively.

2.3. Characterization

Small-angle X-ray scattering (SAXS) measurements were obtained on a Kratky compact small-angle system using Kα radiation at 40 kV and 20 mA, which was equipped with a position-sensitive detector containing 1,024 channels of width 53 mm. The X-ray diffraction (XRD) patterns were measured with a Bruker powder X-ray diffractometer using a Cu radiation source having a wavelength of 1.54 Å ranging from 20° to 80° with a scan speed of 0.04°/s at 40 kV and 40 mA. The surface area of the samples was measured using nitrogen absorption–desorption (BET)-Autosorb-1 from Quantachrome Instruments (US). Prior to the surface area measurements, all samples were degassed at 250°C for 6 h. Transmission electron microscopy (TEM) was carried out using a Philips Tecnai 20 microscope operated at 200 kV.

2.4. Photocatalytic activity measurement

The photoactivity of the resulting materials was measured by degrading the MB dye in an aqueous solution under UV light irradiation (mercury lamp 125 W). All experiments were carried out with a catalyst concentration of 0.3 g/L TiO_2 in 40 mg/L MB. The mixture was first stirred for 30 min in a dark place to achieve the adsorption–desorption equilibrium. The concentration spectrum of the mixture was determined using a UV–Vis spectrometer (in 625 nm wavelength) after centrifuging. The photocatalytic decomposition rate was determined using the following equation [26].

$$\text{Photocatalytic decomposition rate } = \frac{C_0 - C}{C_0} \tag{1}$$

where C_0 is the initial concentration of the MB solution and C is the final concentration after illumination. The decolonization efficiency (%) can be calculated according to the equation:

$$\text{Efficiency } (\%) = \frac{C_0 - C}{C_0} \times 100 \tag{2}$$

3. Results and discussion

Fig. 1(A) shows the XRD pattern of the samples prepared by the introduction of TiO_2 nanoparticles to S70 at different calcination temperatures. As it can be seen, a mixture of the anatase and rutile phase can be achieved simultaneously in all of the samples. It has been reported that the interaction of adjacent rutile and anatase crystals has a positive effect on photocatalytic efficiency [7].

The differences between the rutile and anatase crystals are related to their structure. Regarding anatase structure, the TiO_6 octahedra share faces while edge sharing of octahedra occur in rutile structures [27]. At low synthesis temperatures under acidic conditions, the surface of titania gets protonated and a stable sol is prepared while at higher synthesis temperatures (around 70°C) the nucleus of the rutile crystals take form. At higher pH values, the remaining species of Ti convert into the anatase phase [6,28,29].

Increasing the calcination temperature from 400°C to 800°C appears to create narrower and stronger diffraction peaks, which is a sign of the formation of higher crystallite sizes and degree of crystallinity. The same results can be seen in Fig. 1(B) for samples S130-400 and S130-800. The crystallite size of the prepared samples was calculated using the Scherrer equation [30] from (101) anatase peak or (110) rutile peak which is presented in Table 1. It can be seen that the resulting rutile crystals are larger than the anatase crystals, indicating that large rutile particles can collapse the entrance of the small pores.
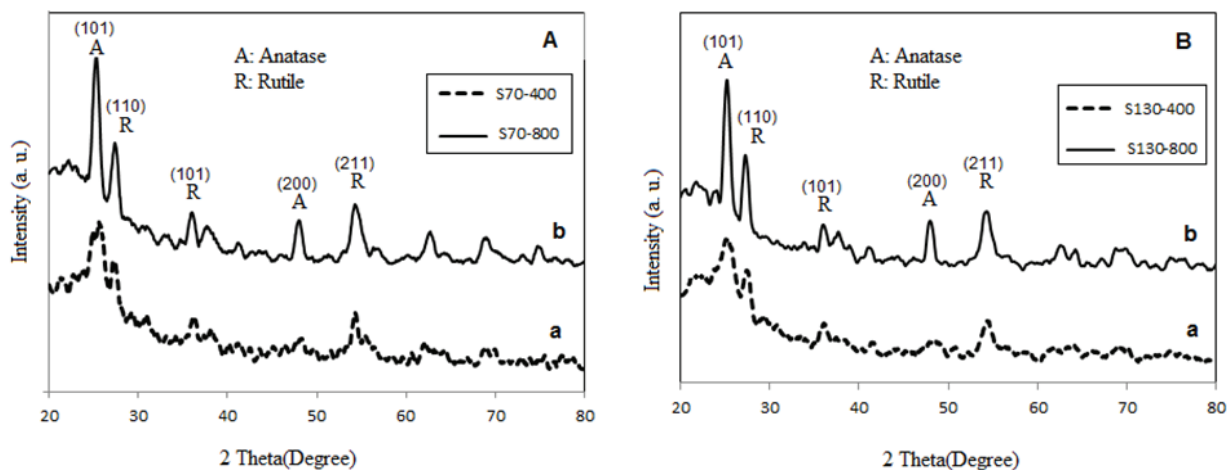
Fig. 1. WAXRD patterns of the samples (A): a, S70-400, b, S70-800 and (B): a, S130-400, b, S130-800.

Table 1
Textural and photocatalytic properties of samples

Sample ID	a_0 (nm)[a]	t (nm)[b]	S_{BET} (m²/g)[c]	V_p (cm³/g)[d]	D_p (nm)[e]	Crystallite size (nm)[f] Anatase	Rutile	K[g] (%)	X_r[h]
S70-400	11.84	6.14	365	0.52	6.2	4.7	7.4	11.7	0.44
S130-400	13.89	2.89	329	0.9	12.6	4.9	7.1	24.2	0.43
S70-800	10.73	4.03	198	0.33	5.6	6.3	10.1	42.5	0.46
S130-800	13.07	2.07	289	0.79	9.9	6.8	9.7	58.1	0.48
S70	11.66	7.06	552	0.67	6.2	–	–	–	–
S130	13.2	2.3	391	1.06	10	–	–	–	–

[a]The unit cell dimension calculated as $(2d_{100}/3^{1/2})$.
[b]Wall thickness estimated as $(a_0 - D_p)$.
[c]Surface area calculated by BET method.
[d]Total pore volume.
[e]Average pore diameter calculated from the adsorption branch by BJH method.
[f]Crystallite size according to Scherrer equation.
[g]Photocatalytic efficiency.
[h]Weight fraction of rutile phase.

The weight fraction of the rutile in the samples was calculated according to Spurr and Myers method [31] (Table 1):

$$X_r = 1 - \left(1 + 1.265\frac{I_r}{I_a}\right)^{-1} \qquad (3)$$

where X_r is the weight fraction of rutile in the sample, and I_r/I_a is the ratio of the intensity of the strongest rutile reflection to the intensity of the strongest anatase reflection. As can be seen in Table 1, the weight fraction of rutile in all of the samples remains almost constant which can be due to the existence of the Ti–O–Si bonds [5,6,32]. These bonds can hinder phase transformation from anatase to rutile at elevated temperatures.

SAXS patterns of S70 and S130 can be seen in Fig. 2(A). Both of the samples (S70 and S130) exhibit three well-resolved diffraction peaks which can be assigned to a two-dimensional hexagonal structure [33]. It is worth mentioning that the appearance of these peaks at low angles is related to the degree of the ordering of pore channels which stems from the electron density difference between the pores and walls. The unit cell parameter of the hexagonal cell, which can be used to calculate the pore-to-pore distance, can be estimated from the spacing of the (100) planes. The achieved results for these samples have been summarized in Table 1. The (110) reflection is stronger for the sample hydrothermal at 130°C

(S130) which could reveal thinner walls [34]. The wall thickness values of the samples are presented in Table 1. Fig. 2(B) shows the SAXS patterns of the samples S70 and S130 after impregnation of TiO$_2$ and a decline in peak intensity can be measured. This suggests that TiO$_2$ particles are deposited inside the pores and on the surface of mesoporous SiO$_2$ structure [35].

The N$_2$ adsorption–desorption isotherms of the prepared samples are shown in Figs. 3(A) and (B).

The related data (surface area S_{BET}, pore volume V_p and pore size D_p) are also presented in Table 1. According to the IUPAC classification, all of the samples are of type IV with a H1 hysteresis loop, which represent a mesoporous structure with one-dimensional cylindrical pores [36].

In Figs. 3(A) and (B), some clear differences can be observed between the N$_2$ sorption results of S70 and S130. Sample S70 shows hysteresis loops at intervals of lower relative pressures ($0.4 < P/P_0 < 0.7$) compared with S130 ($0.7 < P/P_0 < 0.8$) due to a decrease in the size of pore diameter at lower hydrothermal temperatures [37]. Furthermore, the pore volume of S130 is slightly greater than that of S70. On the other hand, S130 has a much lower specific surface area than S70 (Table 1). These differences can be attributed to the hydrophilic nature of poly(ethylene oxide) blocks of the copolymer (P123) at different temperatures [37]. As has been shown in Table 1, both S70-400 and S130-400 show a
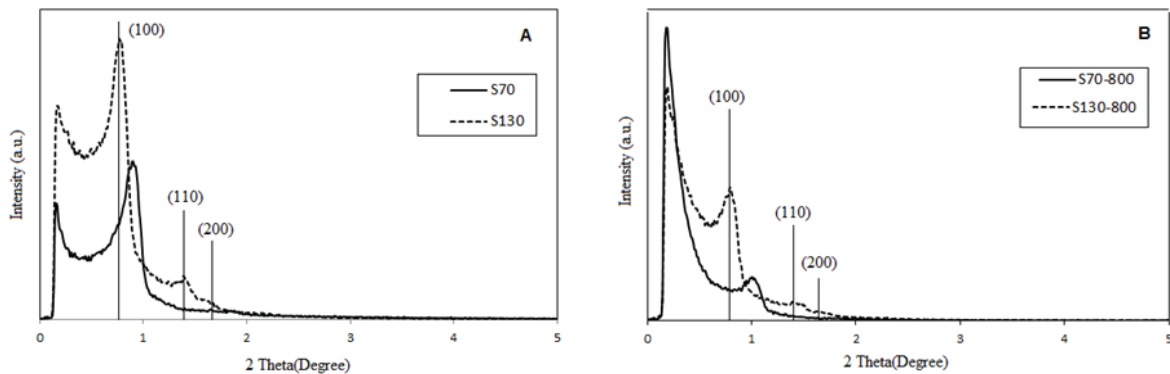
Fig. 2. Small-angle X-ray scattering for samples before (A) and after (B) impregnation and calcination at 800°C.
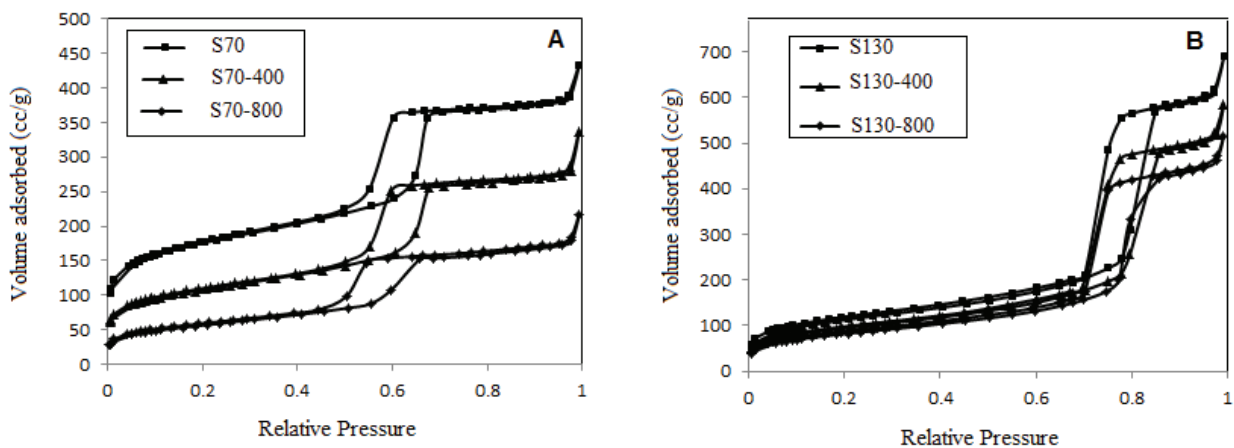
Fig. 3. N$_2$ sorption isotherms of samples: (A) S70 and S70-y, and (B) S130 and S130-y.

reduction in surface area and pore volume compared with S70 and S130, respectively. Although the shape of isotherms of these impregnated samples (S70-400 and S130-400) kept the features of the isotherms exhibited by the unloaded support, small changes in the position and shape can be seen. These small changes, which are due to the introduction of TiO_2 nanoparticles, cause a decrease in surface area and pore volume of samples.

As concluded in Figs. 4(A) and (B), the surface area and pore volume of S70-400 decreased around 34% and 22%, respectively, as compared with the unloaded host structure (S70). The mentioned parameters declined just 16% and 15% for sample S130-400. This dramatic reduction in surface area and pore volume for sample S70-400 compared with S130-400 can be attributed to the pore plugging of small pores of S70 by large rutile particles. Taking into account the opposite surface charge of TiO_2 and mesoporous SiO_2, it is expected that TiO_2 particles deposited on the surface and inside of the pores of the mesoporous structure [18] which have been confirmed by TEM images in Fig. 5. The TEM image shows the hexagonal shape of the pores where the TiO_2 nanoparticles are in the channels and on the pore walls of host structure. EDX analysis of point 1 in Fig. 5(A) also shows a significantly high concentration of Ti.

Small pores of the material can be collapsed simply by large rutile particles which have been shown schematically in Fig. 6. Thus, larger pores can enhance the chances of entering both rutile and anatase particles inside the channels.

In Figs. 4(A) and (B), it is clear that the surface area and pore volume reduction for sample S130-800 are much lower than S70-800. Although S70 has a superior surface area than S130, S70-800 shows a significant lower surface area than S130-800. Increasing the calcination temperature from 400°C to 800°C shows a significant effect on the surface area and pore volume of the samples. In fact, a higher calcination temperature causes a growth of TiO_2 particles and a shrinkage of the mesoporous SiO_2 structure simultaneously. Consequently, some of the pores are closed and this phenomenon is quite likely to happen in small pores.

TiO_2 particles show photocatalytic properties when they are exposed to UV light and they can decompose organic dyes and pollutants like MB into H_2O. The photocatalytic activity of TiO_2 can be related to the creation of photogenerated charge carriers (hole and electron) which occurs upon the absorption of UV light. The generated holes in the valence band diffuse to the TiO_2 surface and react with adsorbed water molecules, forming hydroxyl radicals. The photogenerated holes and the hydroxyl radicals oxidize nearby organic dyes and pollutants on the TiO_2 surface. Meanwhile, electrons in the conduction band typically participate in the reduction processes, which usually reacts with molecular oxygen in the air resulting in the formation of superoxide
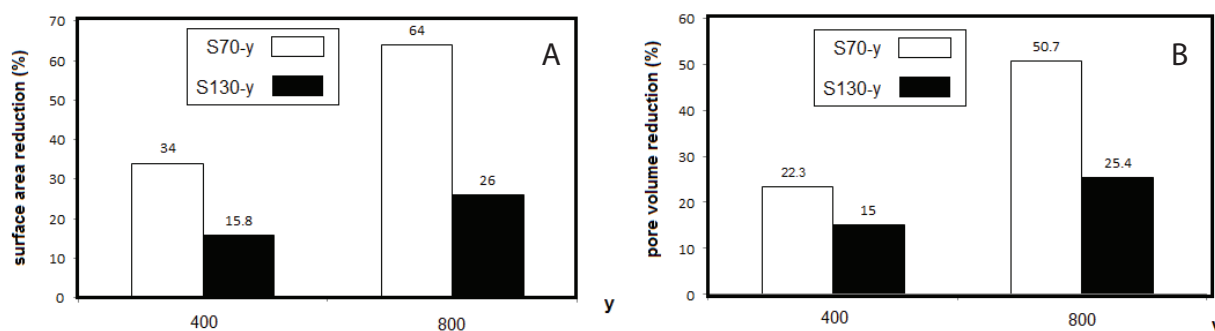
Fig. 4. Surface area reduction percentage (A) and pore volume reduction percentage (B) of impregnated samples relative to unloaded host structures.
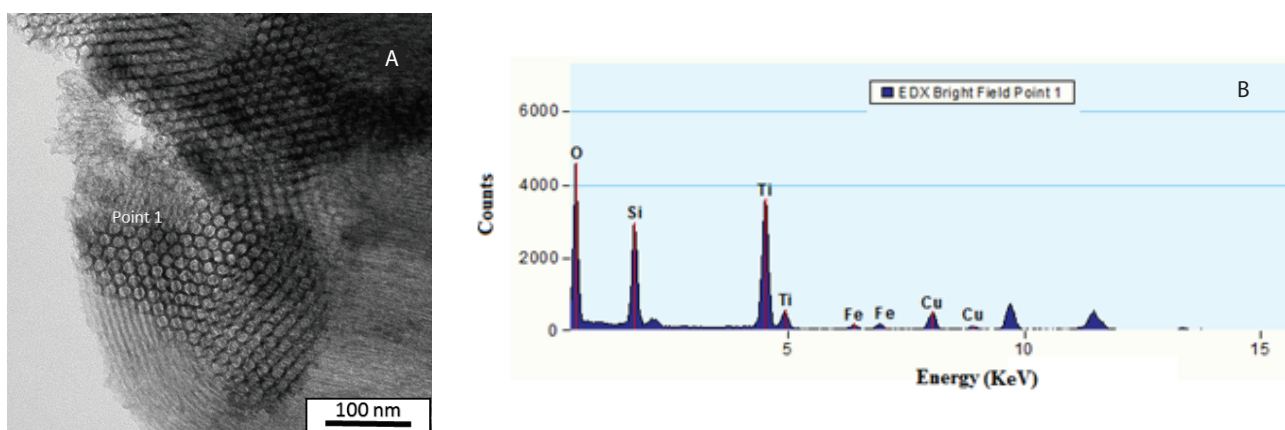
Fig. 5. TEM image of sample S130-400 (A) and EDX spectra of point 1 (B).

radical anions [38]. The photocatalytic efficiency of TiO_2 will depend upon several factors including particle size, specific surface area, porosity, crystalline phase (anatase or rutile) and crystallinity [5,6,32,39]. In addition, it is known that the coexistence of rutile and anatase leads to an increased photocatalytic activity [7].

The photocatalytic degradation of MB solution under UV light irradiation has been used to evaluate the photocatalytic efficiency of the prepared mesostructured TiO_2–SiO_2 samples and the results have been presented in Fig. 7. Pure commercial TiO_2 nanoparticles (P25, BET = 50 m^2/g, Degussa Co.) were tested to compare their photoactivity value in the same system and with the same amount of TiO_2. In MB degradation tests, surface adsorption and photodegradation of the samples are the parameters responsible for the decrease in the concentration of MB [40], so the samples had to be stirred in a dark place for 30 min and were then exposed to UV light in order to estimate photoactivity of the samples precisely.

According to the achieved results in Fig. 7 and Eq. 2, the photodegradation efficiency of the prepared samples between 30 and 105 min are also shown in Table 1. It can be seen that the samples S70-400 and S130-400 decreased the concentration of MB by 11.7% and 24.2%, respectively and these estimated values are lower than the degradation of commercial TiO_2 (P25) with 28.3%. Low photocatalytic efficiency of these samples

compared with P25 can be related to the low degree of crystallinity of these samples because of a low calcination temperature [5]. Regarding the photoactivity of S70-400 and S130-400, two effective parameters including SiO_2 mesostructure pore size and surface area should be considered. As large pores of host structures are much more accessible, TiO_2 particles can be impregnated into them easily. In addition, these large pores cannot be plugged with ease. According to the achieved results in Table 1, it is clear that unlike S130, the pore size of S70 is smaller than rutile crystals, so only anatase particles can enter into its channels (Fig. 6). On the other hand, as photodegradation of dyes is a surface reaction, a higher surface area can prepare more photoactive places and it can increase photodegradation efficiency. Therefore, although surface area of S70-400 is higher than S130-400, it shows photoactivity half as big as S130-400 because of the accessible pores of S130-400. When the calcination temperature rises from 400°C to 800°C, TiO_2 nanoparticles grow and the SiO_2 mesostructure shrinks, which results in additional plugging and leads to a reduction in surface area, total pore volume and consequently photoactivity. On the other hand, a higher calcination temperature can cause a significant improvement in the degree of crystallinity of TiO_2 which results in a dramatic increase in photoactivity. Therefore, the photocatalytic degradation of S70-800 and S130-800 has jumped dramatically by 42.5% and 57%,
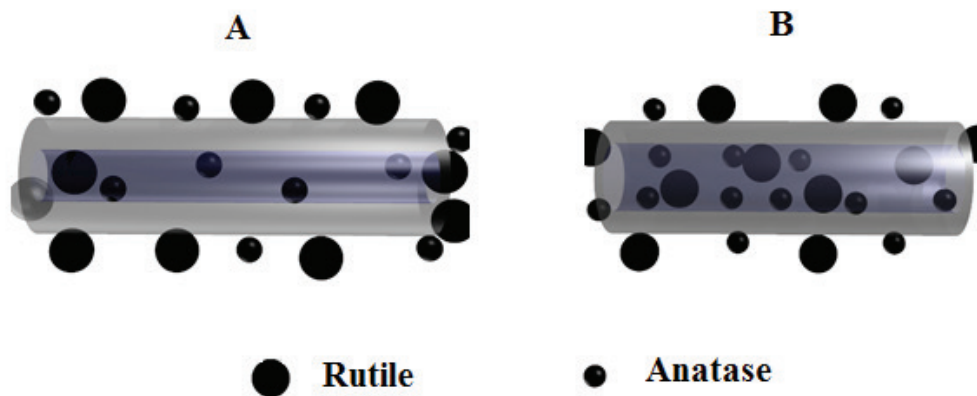
Fig. 6. Schematic illustration of the interaction of rutile and anatase crystals with samples S70 (A) and S130 (B).
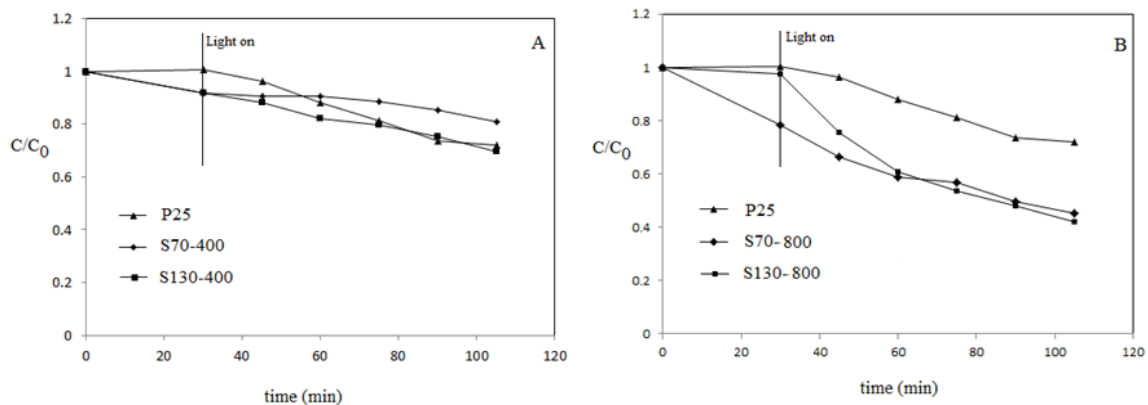
Fig. 7. Photocatalytic decomposition of methyl blue on samples Sx-400 (A) and Sx-800 (B).

respectively. Interestingly, although S70 shows a higher surface area than S130, the surface area and photodegradation efficiency of S130-800 present a superior value compared with S70-800 owing to bigger and more available channels of S130.

4. Conclusions

In this study, mesoporous SiO_2 with two different pore sizes were synthesized. TiO_2 nanoparticles including rutile and anatase were then introduced to mesoporous SiO_2 host structures. The results showed that pore size of mesoporous SiO_2 has a significant effect on physical properties and the photoactivity of prepared SiO_2–TiO_2 materials. In fact, the chances of impregnation of both rutile and anatase phases into larger pores are much more feasible, and consequently it has a positive effect on photocatalytic properties on synthesized samples. In addition, samples with larger channels retained surface area at high calcination temperatures because bigger pores are more likely to stay open and accessible at elevated temperatures.

Acknowledgments

References

[1] J. Schneider, M. Matsuoka, M. Takeuchi, J. Zhang, Y. Horiuchi, M. Anpo, D.W. Bahnemann, Understanding TiO_2 photocatalysis: mechanisms and materials, Chem. Rev., 114 (2014) 9919–9986.

[2] S.M. Ibrahim, N. Negishi, A.K. Masrom, B. Mazinani, A. Ramli, A. Isnin, M.Z. Abdul Malek, TiO_2 transparent thin film for eliminating toluene, ISRN Nanotechnol., 2012 (2012) 1–9.

[3] M. Machida, K. Norimoto, T. Watanabe, K. Hashimoto, A. Fujishima, The effect of SiO_2 addition in super-hydrophilic property of TiO_2 photocatalyst, J. Mater. Sci., 34 (1999) 2569–2574.

[4] J.-G. Yu, H.-G. Yu, B. Cheng, X.-J. Zhao, J.C. Yu, W.-K. Ho, The effect of calcination temperature on the surface microstructure and photocatalytic activity of TiO_2 thin films prepared by liquid phase deposition, J. Phys. Chem. B., 107 (2003) 13871–13879.

[5] B. Mazinani, A. Beitollahi, A.K. Masrom, N. Yahya, T.S.Y. Choong, S.M. Ibrahim, J. Javadpour, Characterization and evaluation of the photocatalytic properties of wormhole-like mesoporous silica incorporating TiO_2, prepared using different hydrothermal and calcination temperatures, Res. Chem. Intermed., 38 (2012) 1733–1742.

[6] B. Mazinani, A.K. Masrom, A. Beitollahi, R. Luque, Photocatalytic activity, surface area and phase modification of mesoporous SiO_2–TiO_2 prepared by a one-step hydrothermal procedure, Ceram. Int., 40 (2014) 11525–11532.

[7] T. Ohno, K. Sarukawa, K. Tokieda, M. Matsumura, Morphology of a TiO_2 photocatalyst (Degussa, P-25) consisting of anatase and rutile crystalline phases, J. Catal., 203 (2001) 82–86.

[8] A. Testino, I.R. Bellobono, V. Buscaglia, C. Canevali, M. D'Arienzo, S. Polizzi, R. Scotti, F. Morazzoni, Optimizing the photocatalytic properties of hydrothermal TiO_2 by the control of phase composition and particle morphology. A systematic approach, J. Am. Chem. Soc., 129 (2007) 3564–3575.

[9] C. Reitz, J. Reinacher, P. Hartmann, T. Brezesinski, Polymer-templated ordered large-pore mesoporous anatase–rutile TiO_2: Ta nanocomposite films: microstructure, electrical conductivity, and photocatalytic and photoelectrochemical properties, Catal. Today, 225 (2014) 55–63.

[10] G.J. de A.A. Soler-Illia, A. Louis, C. Sanchez, Synthesis and characterization of mesostructured titania-based materials through evaporation-induced self-assembly, Chem. Mater., 14 (2002) 750–759.

[11] S.M. Ibrahim, A.K. Masrom, B. Mazinani, S. Radiman, F.M. Jamil, A. Beitollahi, N. Negishi, N. Yahya, Mesoporous titania photocatalyst: effect of relative humidity and aging on the preparation of mesoporous titania and on its photocatalytic activity performance, Res. Chem. Intermed., 39 (2013) 1003–1014.

[12] Y. Xu, C.H. Langford, UV-or visible-light-induced degradation of X3B on TiO_2 nanoparticles: the influence of adsorption, Langmuir, 17 (2001) 897–902.

[13] T. Torimoto, Y. Okawa, N. Takeda, H. Yoneyama, Effect of activated carbon content in TiO_2-loaded activated carbon on photodegradation behaviors of dichloromethane, J. Photochem. Photobiol., A, 103 (1997) 153–157.

[14] J. Klaas, G. Schulz-Ekloff, N.I. Jaeger, UV-visible diffuse reflectance spectroscopy of zeolite-hosted mononuclear titanium oxide species, J. Phys. Chem., B, 101 (1997) 1305–1311.

[15] S. Fukahori, H. Ichiura, T. Kitaoka, H. Tanaka, Photocatalytic decomposition of bisphenol A in water using composite TiO_2-zeolite sheets prepared by a papermaking technique, Environ. Sci. Technol., 37 (2003) 1048–1051.

[16] C.T. Kresge, M.E. Leonowicz, W.J. Roth, J.C. Vartuli, J.S. Beck, Ordered mesoporous molecular sieves synthesized by a liquid-crystal template mechanism, Nature, 359 (1992) 710–712.

[17] Z. Luan, E.M. Maes, P.A.W. Van der Heide, D. Zhao, R.S. Czernuszewicz, L. Kevan, Incorporation of titanium into mesoporous silica molecular sieve SBA-15, Chem. Mater., 11 (1999) 3680–3686.

[18] E. Beyers, E. Biermans, S. Ribbens, K. De Witte, M. Mertens, V. Meynen, S. Bals, G. Van Tendeloo, E.F. Vansant, P. Cool, Combined TiO_2/SiO_2 mesoporous photocatalysts with location and phase controllable TiO_2 nanoparticles, Appl. Catal., B, 88 (2009) 515–524.

[19] C. Anderson, A.J. Bard, An improved photocatalyst of TiO_2/SiO_2 prepared by a sol-gel synthesis, J. Phys. Chem., 99 (1995) 9882–9885.

[20] R.N. Viswanath, S. Ramasamy, Study of TiO_2 nanocrystallites in TiO_2-SiO_2 composites, Colloids Surf., A, 133 (1998) 49–56.

[21] Z.F. Liu, J. Tabora, R.J. Davis, Relationships between microstructure and surface acidity of Ti-Si mixed oxide catalysts, J. Catal., 149 (1994) 117–126.

[22] R. Poliah, S. Sreekantan, Characterization and photocatalytic activity of enhanced copper-silica-loaded titania prepared via hydrothermal method, J. Nanomater., 2011 (2011) 1–8.

[23] R. Su, R. Bechstein, L. So, R.T. Vang, M. Sillassen, B. Esbjornsson, A. Palmqvist, F. Besenbacher, How the anatase-to-rutile ratio influences the photoreactivity of TiO2, J. Phys. Chem. C., 115 (2011) 24287–24292.

[24] W.-K. Wang, J.-J. Chen, X. Zhang, Y.-X. Huang, W.-W. Li, H.-Q. Yu, Self-induced synthesis of phase-junction TiO_2 with a tailored rutile to anatase ratio below phase transition temperature, Sci. Rep., 6 (2016) 1–10.

[25] A. Bhattacharyya, S. Kawi, M.B. Ray, Photocatalytic degradation of orange II by TiO_2 catalysts supported on adsorbents, Catal. Today, 98 (2004) 431–439.

[26] K.H. Yoon, J.S. Noh, C.H. Kwon, M. Muhammed, Photocatalytic behavior of TiO_2 thin films prepared by sol–gel process, Mater. Chem. Phys., 95 (2006) 79–83.

[27] S. Yin, R. Li, Q. He, T. Sato, Low temperature synthesis of nanosize rutile titania crystal in liquid media, Mater. Chem. Phys., 75 (2002) 76–80.

[28] Q.H. Zhang, L. Gao, J.K. Guo, Preparation and characterization of nanosized TiO_2 powders from aqueous $TiCl_4$ solution, Nanostruct. Mater., 11 (1999) 1293–1300.

[29] K. Yanagisawa, J. Ovenstone, Crystallization of anatase from amorphous titania using the hydrothermal technique: effects of starting material and temperature, J. Phys. Chem. B, 103 (1999) 7781–7787.

[30] A.L. Patterson, The Scherrer formula for X-ray particle size determination, Phys. Rev., 56 (1939) 978.

[31] R.A. Spurr, H. Myers, Quantitative analysis of anatase-rutile mixtures with an X-ray diffractometer, Anal. Chem., 29 (1957) 760–762.

[32] B. Mazinani, A. Beitollahi, S. Radiman, A.K. Masrom, S.M. Ibrahim, J. Javadpour, F.M.D. Jamil, The effects of hydrothermal temperature on structural and photocatalytic properties of ordered large pore size TiO_2–SiO_2 mesostructured composite, J. Alloys Compd., 519 (2012) 72–76.

[33] D. Zhao, J. Feng, Q. Huo, N. Melosh, G.H. Fredrickson, B.F. Chmelka, G.D. Stucky, Triblock copolymer syntheses of mesoporous silica with periodic 50 to 300 angstrom pores, Science, 279 (1998) 548–552.

[34] B.P. Feuston, J.B. Higgins, Model structures for MCM-41 materials: a molecular dynamics simulation, J. Phys. Chem., 98 (1994) 4459–4462.

[35] K. Su, Z. Li, B. Cheng, D. Shen, Y. Wang, Studies on the carboxymethylation and methylation of bisphenol A with dimethyl carbonate over TiO_2/SBA-15, J. Mol. Catal. A: Chem., 315 (2010) 60–68.

[36] G. Leofanti, M. Padovan, G. Tozzola, B. Venturelli, Surface area and pore texture of catalysts, Catal. Today, 41 (1998) 207–219.

[37] G.J. de AA Soler-Illia, E.L. Crepaldi, D. Grosso, C. Sanchez, Block copolymer-templated mesoporous oxides, Curr. Opin. Colloid Interface Sci., 8 (2003) 109–126.

[38] A. Fujishima, T.N. Rao, D.A. Tryk, Titanium dioxide photocatalysis, J. Photochem. Photobiol., C, 1 (2000) 1–21.

[39] Q.-Z. Yan, X.-T. Su, Z.-Y. Huang, C.-C. Ge, Sol–gel auto-igniting synthesis and structural property of cerium-doped titanium dioxide nanosized powders, J. Eur. Ceram. Soc., 26 (2006) 915–921.

[40] D.R. Sahu, L.Y. Hong, S.-C. Wang, J.-L. Huang, Synthesis, analysis and characterization of ordered mesoporous TiO_2/SBA-15 matrix: effect of calcination temperature, Microporous Mesoporous Mater., 117 (2009) 640–649.